Eleventh South African Conference on Computational and Applied Mechanics
SACAM 2018
Vanderbijlpark, South Africa, 17-19 September 2018

Implementation of a visco-plastic sea ice model into OpenFOAM

Alfred E J Bogaers[a], Gerhardus J Jansen van Rensburg[b], Rutger Marquart[c], Sebastian Skatulla[c]

[a,b] *Advanced Mathematical Modelling, Modelling and Digital Science, Council for Scientific and Industrial Research, Pretoria, South Africa*
[a,b] *Computer Science and Applied Mathematics, University of the Witwatersrand, Johannesburg, South Africa*
[c] *Department of Civil Engineering, University of Cape Town, Rondebosch, Cape Town, South Africa*

email address : abogaers@csir.co.za[a]

Abstract

In this paper, we outline the implementation of Hibler's visco-plastic (VP) sea ice model into OpenFOAM, an open-source finite-volume modelling toolkit. Hibler's visco-plastic model is arguably the most widely used description of sea ice rheology, and finds application in most global climate models. The VP model has been shown to accurately capture the bulk behaviour of sea ice at large length scales. Under convergent conditions, the VP model allows the sea ice to deform plastically, while for small strains, near drift like conditions can be captured. Unfortunately however, due to the potential for large viscosities, the VP model tends to become numerically unstable. The general consensus in literature is that an implicit solution scheme is required, which tend to become expensive when used in global climate models. Suggestions to improve the convergence behaviour include techniques such as successive over-relaxation or via the addition of an elastic term, known as the elastic-visco-plastic (EVP) method. In this paper, we aim introduce the concept of dynamic relaxation, which in addition to matrix conditioning, can be used to both stabilise and accelerate the iterative convergence behaviour. The behaviour of the sea ice model will be demonstrated on a number of test cases.

Keywords: sea ice modelling, OpenFOAM, visco-plastic rheology, dynamic relaxation

1. Introduction

Sea ice plays an important role in global climate. It influences the global ocean circulation, and affects global climate due to its inherent reflective nature. In most models used to study long term climate change, sea ice is often treated rather simplistically. With the advances in sea ice models, and numerical solution schemes, modern sea ice models have become far more comprehensive.

Sea ice is a heterogeneous, anisotropic material, and generally forms a highly fractured surface with various ice flow shapes and sizes. The local distribution of ice-thickness, floe sizes and lead fractions varies across the various Polar Regions. In order to directly model such a system would require computational models at length scales in the order of a few meters, making them computationally infeasible for global climate models.

It is by now generally accepted that sea ice at large length scales, in the order of 10 to 100kms, can be appropriately described as a continuum medium. Pack ice behaviour on large scales has been observed to have a low tensile strength, supports shear stresses and has a maximum compressive strength related to ice thickness and fractional coverage. Many models have been developed to describe the ice dynamics. Early studies focused on free drift descriptions with no ice interaction (see for example [1]). In free drift descriptions, ice is allowed to move freely as a function of external forces until the ice reaches a certain height or mass, or encounters land, and is forced to stop. Other ice rheologies included treating ice as a Newtonian viscous fluid [2], a linear viscous fluid, cavitating flow [3] or a plastic material model. A nonlinear visco-plastic (VP) model first proposed by Hibler [4] has largely been established as the standard sea ice dynamics model, and forms the basis for most of the recent sea ice studies.

2. Sea ice flow model

Pack ice typically consists of rigid plates, which may drift freely in areas of relatively open water or be closely packed together in regions of high ice concentration. Although individual ice floes range from tens of meters to several kilometres across, the ice pack can be considered as a highly fractured two-dimensional continuum.

In two dimensional Cartesian co-ordinates, the force balance on the ice, per unit area, is given by

$$\frac{\partial m\boldsymbol{U}}{\partial t} + \nabla \cdot (m\boldsymbol{U}\boldsymbol{U}) = \boldsymbol{\tau}_a + \boldsymbol{\tau}_w + \nabla \cdot \boldsymbol{\sigma}, \tag{1}$$

where m is the ice mass, $\boldsymbol{U}$ is the ice velocity, $\boldsymbol{\tau}_a$ and $\boldsymbol{\tau}_w$ are the wind and ocean stresses on the ice respectively and $\nabla \cdot$ indicates the divergence operator. The remaining term, $\nabla \cdot \boldsymbol{\sigma}$, represents the internal stress state, which depends on the chosen flow rheology to describe the sub-scale interactions between the ice floes.

By scale analysis, it has shown that the advection of the momentum term, $\nabla \cdot (m\boldsymbol{U}\boldsymbol{U})$, is sufficiently small to be neglected (see for example [4]). While many studies do in fact ignore the inertial component, we retain the term within the present study for numerical reasons.

The wind, τ_a, and ocean stresses, τ_w, are typically modeled with a quadratic boundary layer model which can be defined as [5,6]

$$\boldsymbol{\tau}_a = \rho_a C_a |\boldsymbol{U}_a| (\boldsymbol{U}_a \cos\theta_a + \boldsymbol{k} \times \boldsymbol{U}_a \sin\theta_a), \tag{2}$$

$$\boldsymbol{\tau}_w = \rho_w C_w |\boldsymbol{U}_w - \boldsymbol{U}| \big((\boldsymbol{U}_w - \boldsymbol{U}) \cos\theta_w + (\boldsymbol{U}_w - \boldsymbol{U})\boldsymbol{k} \times \sin\theta_w \big). \tag{3}$$

The drag laws require that the air velocity, $\boldsymbol{U}_a$, above the atmospheric boundary layer and the ocean currents, $\boldsymbol{U}_w$, below the surface Ekman layer be known. The other variables include air and water densities, ρ_a and ρ_w, turning angles across the boundary layers, θ_a and θ_w and the drag coefficients for the air and water interfaces given by C_a and C_w. Lastly, $\boldsymbol{k}$ is the unit normal vector to the sea ice surface, and × indicates the cross-product.

While many studies distinguish between thin and thick ice, as well as often including snow cover, for the current study, we limit our ice mass to

$$m = \rho_i h, \tag{4}$$

where ρ_i is the ice density and h is the effective sea ice height.

3. Sea ice Rheology

The non-linear, visco-plastic model (VP) model, first proposed by Hibler [4], has since become the standard, large scale, sea ice model. The VP rheology provides a relationship between internal ice stress $\boldsymbol{\sigma}$ and strain rates $\dot{\boldsymbol{\epsilon}}$ through an internal ice strength$P$, and bulk and shear viscosities, ζ and η respectively. The visco-plastic formulation is posed such that the principle components of stress lie on an elliptic yield curve, with a ratio $e = 2$ between the major and minor axes.

The VP description allows the ice pack to diverge with little or no stress, yet resist compression and shearing motion under convergent conditions. The internal ice stress state is defined as

$$\boldsymbol{\sigma} = 2\eta\dot{\epsilon} + \boldsymbol{I}\left[(\zeta - \eta)\mathrm{tr}(\dot{\epsilon}) - \frac{P}{2}\right], \tag{5}$$

where $\boldsymbol{I}$ is the identity matrix and

$$\dot{\boldsymbol{\epsilon}} = \frac{1}{2}(\nabla\boldsymbol{U} + \nabla\boldsymbol{U}^T). \tag{6}$$

The bulk (ζ) and shear (η) viscosities are given by

$$\zeta = \frac{P}{2\Delta}, \tag{7}$$

$$\eta = \frac{P}{2\Delta e^2}, \tag{8}$$

where Δ is defined by

$$\Delta = \left[(\dot{\epsilon}^2{}_{11} + \dot{\epsilon}^2{}_{22})(1 + e^{-2}) + 4e^{-2}\dot{\epsilon}^2{}_{12} + 2\dot{\epsilon}_{11}\dot{\epsilon}_{12}(1 - e^{-2})\right]^{1/2}. \tag{9}$$

To close of the system of equations requires some definition for the ice strength, P. Hibler [4] proposed a simple relationship based on compactness and thickness

$$P = P^* hAe^{-C(1-A)}, \tag{10}$$

where P^* and C are empirical constants and A represents the surface area fraction (fraction of control volume covered by ice).

As strain rates approach zero, the viscosities η and ζ tend to infinity. Hibler proposed regularizing this behavior by posing an upper bound on the allowable viscosities such that

$$\zeta_{\max} = 2.5 \times 10^8 P, \quad \text{and} \quad \eta_{\max} = \frac{\zeta_{\max}}{e^2}. \tag{11}$$

3.1. Ice Transport

The evolution of effective ice thickness, h, and fractional ice coverage, A, is defined as:

$$\frac{\partial h}{\partial t} = \nabla \cdot (h\boldsymbol{U}) = S_h \tag{12}$$

$$\frac{\partial A}{\partial t} = \nabla \cdot (A\boldsymbol{U}) = S_A \tag{13}$$

Where S_A and S_h are the thermodynamic source terms defining growth/melt of sea ice. The thermodynamic source terms can either be based on interpolated values such as those presented in [7] or from a thermodynamic, phase change model. For the purposes of this paper we assume both thermodynamic source terms to be 0 ($S_A = 0$ and $S_h = 0$).

From a physical perspective values for h and A have natural bounds. Effective sea ice height $h \geq 0$, where $h = 0$ and $A = 0$ would indicate a region of no ice. Sea ice coverage fraction is also naturally bounded by $0 \leq A \leq 1$. Equations (12) and (13) naturally guarantee that both $h \geq 0$ and $A \geq 0$, however, it is possible for A to be larger than 1. As suggested in [4], we limit A by capping $A = 1$ as an upper limit, i.e. whenever a value of $A > 1$ is computed within a cell that same cell value is reset to 1. While no issues have been raised by imposing an upper limit on A in this fashion, numerical instabilities may arise.

4. Numerical Implementation

4.1. Numerical Solution

The model was implemented into OpenFOAM and is therefore based on the finite-volume method for co-located grids, suited to non-orthogonal, arbitrary meshes. A staggered solution approach is used, where the cross-coupling terms are lagged. The chosen approach is similar to the strength explicit scheme of Hutchings *et al.* [8] and the implicit visco-plastic solvers discussed in [9, 10].

The model consists of the following solution sequence:

a) Calculate the melt/growth rates (set to 0 for the purposes of this paper).

b) Solve: $\frac{\partial h}{\partial t} + \nabla \cdot (h\boldsymbol{U}) = S_h$

c) Solve: $\frac{\partial A}{\partial t} + \nabla \cdot (A\boldsymbol{U}) = S_A$

d) Compute ζ, η and P based on the current guesses of $\boldsymbol{U}$, h and A using equations (7)-(11).

e) Solve: $\frac{\partial m\boldsymbol{U}}{\partial t} + \nabla \cdot (m\boldsymbol{U}\boldsymbol{U}) = \boldsymbol{\tau}_a + \boldsymbol{\tau}_w + \nabla \cdot \boldsymbol{\sigma}$

f) Iterate through steps d) and e) until convergence.

g) Proceed to the next time step.

While the solver is classifiable as a staggered or a partitioned solution approach, each of the equations are solved implicitly, allowing for much larger time steps than typically used in literature for sea ice models [4,8,11]. In other words, for each of the solution steps b.) through e.) a linear system of the form

$$\boldsymbol{M}x = b, \tag{14}$$

is constructed and solved using a matrix free, Newton-Krylov solution method.

Matrix $\boldsymbol{M}$ refers to a sparsely populated, diagonally dominant matrix. In the discussions to follow, we make distinctions between treating terms as implicit or explicit. By implicit we mean to imply that the given term will be

included within matrix $\boldsymbol{M}$ where explicit terms are in turn included as a source within vector b. This system is then iterated on until the convergence criterion is satisfied.

The sea ice velocities are comparatively low, and therefore we only iteratively couple the sea ice strength and momentum equations (namely solution steps d. and e.), where the primary variables h, A and $\boldsymbol{U}$ are loosely coupled in time.

4.2. Matrix conditioning and dynamic relaxation

The momentum equation (1) with a visco-plastic flow rheology presents a surprisingly difficult equation to solve. This is evidenced by the sheer number of proposed solution methodologies, ranging from dual time stepping methods [4], line over-relaxation with a tri-diagonal system solution matrices [11, 12] and variations thereof [8 ,9 ,10, 13, 14].

Hunke *et al.* [11] introduced an elastic-visco-plastic (EVP) model, where an additional elastic term is included within the momentum equation. The EVP method was introduced to allow for an explicit like discretization of the momentum equation by including an additional elastic term and sub-cycling within each time step. The EVP method has shown enormous potential, and has therefore been widely adopted by the sea ice community. There have, however, been studies that have shown that the explicit EVP and implicit VP solutions can differ significantly [9,10], where the EVP method can take longer to converge to the VP solution, or sometimes leads to solutions with lower than intended viscosities.

We have therefore opted for an implicit solution of the VP momentum equation, in line with the strength-explicit algorithm defined in [8]. We employ an iterative solution method, where a portion of the momentum equation is treated implicitly, and hence included in the linear system matrix $\boldsymbol{M}$, with the remaining portion treated as source terms.

In Hutchings [13], it was shown that the linear system

$$\nabla \cdot \boldsymbol{\sigma} = \underbrace{\nabla \cdot (\eta \nabla \boldsymbol{U})}_{\text{implicit}} + \underbrace{\nabla \cdot \left[(\zeta - \eta) \boldsymbol{I} \text{tr}(\nabla \boldsymbol{U}) + \nabla \cdot (\eta \nabla \boldsymbol{U}^T) - \frac{\nabla P}{2} \right]}_{\text{explicit}}, \tag{15}$$

can be stabilized through the addition of $\nabla \cdot (\zeta \nabla \boldsymbol{U})$ such that the discretization of the stress constitutive term becomes

$$\nabla \cdot \boldsymbol{\sigma} = \underbrace{\nabla \cdot \big((\eta + \zeta) \nabla \boldsymbol{U} \big)}_{\text{implicit}} + \underbrace{\nabla \cdot \left[(\zeta - \eta) \boldsymbol{I} \text{tr}(\nabla \boldsymbol{U}) + \nabla \cdot (\eta \nabla \boldsymbol{U}^T) - \nabla \cdot (\zeta \nabla \boldsymbol{U}) - \frac{\nabla P}{2} \right]}_{\text{explicit}}. \tag{16}$$

For the remainder of the paper we will refer to this as matrix conditioning. The reasoning stems from, if only $\nabla \cdot (\eta \nabla \boldsymbol{U})$ is entered into the linear system matrix $\boldsymbol{M}$, then the explicit portion of the diffusion is larger than the implicit component, and in turn the solution is driven by the set of explicit source terms.

In Zhang and Hibler [12] an over-relaxation predictor-corrector type scheme was proposed. The primary concern with relaxation schemes is that they require an upfront choice on the relaxation parameter, which typically involves problem specific tuning. We therefore propose the use of Aitken's dynamic relaxation [15, 16], which has found wide spread use within the partitioned fluid-structure interactions community. To briefly outline Aitken's method, consider that two iterates within a given time step have been completed. It is then possible to construct a solution residual

$$\boldsymbol{r}_k = \boldsymbol{U}_k - \boldsymbol{U}_{k-1}, \tag{17}$$

where k indicates the current coupling iteration count.

Given a relaxation factor ω, the velocity update can be stabilized by

$$\boldsymbol{U}_k = \boldsymbol{U}_k + \omega \boldsymbol{r}_k. \tag{18}$$

Aitken's dynamic relaxation defines an update rule to dynamically modify the relaxation parameter using the residual results from two previous iterations such that

$$\omega_{k+1} = -\omega_k \frac{(\boldsymbol{r}_{k-1}) \cdot (\boldsymbol{r}_k - \boldsymbol{r}_{k-1})}{(\boldsymbol{r}_k - \boldsymbol{r}_{k-1}) \cdot (\boldsymbol{r}_k - \boldsymbol{r}_{k-1})}. \tag{19}$$

Aitken's method can be shown to fall within the family of least change secant methods [17].

To illustrate the effect of matrix conditioning, as well as the potential benefits of Aitken's method, consider the convergence plot shown here in Figure 1, for the first iteration of the benchmark problem outlined in Section 5.1. The convergence plots clearly show that the matrix conditioning introduced in [8] and [13] does assist with the iterative coupling. Aitken's dynamic relaxation can further be shown to accelerate the overall convergence behaviour. Hutchings [13] employed a fixed number of iterations, typically in the order of 10 iterations per time step. For the remainder of the paper we iterate until the convergence criteria of $\boldsymbol{r}_{\text{relative}} \leq 1 \times 10^{-4}$ is satisfied, which depending on the complexity of the problem, and the time step size, generally falls in the range of 2-40 iterations within any given time step.

4.3. Treatment of regions without ice

Typically, in regions where there is no ice, hence 0 mass, the momentum equation becomes ill-posed (infinite possible velocities). To solve this, Hibler [4] proposed using a two level sea ice thickness description, where a distinction is made between thin ice h and thick ice H such that the sea ice mass becomes

$$m = \rho_i[cH + (1-c)h]. \tag{20}$$

h in this case represents a lower limit on sea ice height, and carries no strength. Hutchings [13] for example enforces a lower limit of $h = 0.5$m, which is considered as thin ice and carries no strength.

Instead of imposing a lower limit on sea ice height, we treat a portion of the water shear stress $\boldsymbol{\tau}_w$ $\boldsymbol{t}_w$ implicitly such that

$$\boldsymbol{\tau}_w = \underbrace{-\rho_w C_w |\boldsymbol{U}_w - \boldsymbol{U}| \cos\theta_w \boldsymbol{U}}_{\text{semi-implicit}} + \underbrace{\rho_w C_w |\boldsymbol{U}_w - \boldsymbol{U}| (\boldsymbol{U}_w \cos\theta + (\boldsymbol{U}_w - \boldsymbol{U})\, \boldsymbol{k} \times \sin\theta_w)}_{\text{explicit}}. \tag{21}$$

In this way, we ensure in the special case of $m = 0$, the mean velocity will be the velocity which satisfies $\boldsymbol{\tau}_a + \boldsymbol{\tau}_w = 0$ or $\rho_a C_a |\boldsymbol{U}_a| \boldsymbol{U}_a = \rho_w C_w |\boldsymbol{U}| \boldsymbol{U}$.

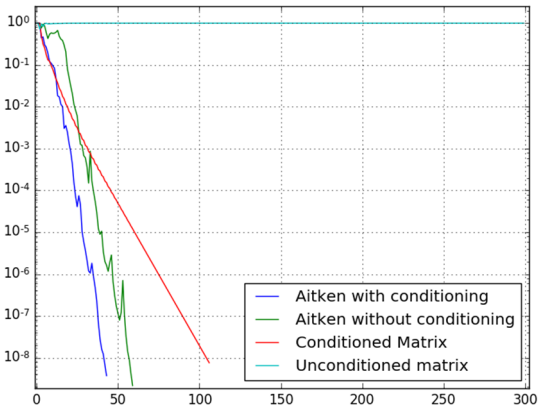

Fig. 1: Illustrative comparison of the convergence rates when using matrix conditioning as well as Aitken's dynamic relaxation.

By implicit we once again mean to imply that the term in question is included within the matrix corresponding to the linear system in equation (14).

5. Test Problems

In the sections to follow, we illustrate the behaviour of the sea ice model on two benchmark problems. For both test cases, implicit Euler time integration is used, where a van Leer's total variation diminishing (TVD) [18] scheme is used for the advection terms in equations (12) and (13), and standard upwinding for all the other advection terms. TVD schemes allows one to better capture sharp interfaces (without any spurious oscillations) which may exist between regions of sea ice and open water, which is especially important for the test problem in Section 5.2. The height and surface fraction equations are solved using a preconditioned conjugate gradient solver, where a generalised algebraic multi-grid solver, with incomplete LU factorisation, is used for the momentum equation.

5.1. 1D convergent/divergent test problem

We reproduce here a simple 1D convergent-divergent test problem introduced in [13]. The test problem consists of a 3000km long ocean region covered completely by ice with h_0 = 1m and A_0 = 1 with the ice initially at rest, $\boldsymbol{U}_0$ = 0ms^{-1}. The 3000km region is split into 100km equally sized control volumes, with an imposed wind velocity of 3m/s from left to right in the *x*-direction. The problem is illustratively shown in Figure 2. To constrain the flow in the *x*-direction, Coriolis force and the water and air turning angles are set to 0. The sea ice simulation parameters are summarized in Table 1, and we make use of time step sizes of Δt = 1 day.

The sea ice strength parameter and air velocity is chosen such that open water forms on the left hand boundary and the ice converges onto the right boundary. To illustrate this we show the sea ice velocity and sea ice height after 1 year of integration in Figure 3. In the diverging region on the left hand side, when sea ice mass goes to zero, $m \to 0$, the momentum equation based on the semi-implicit treatment of the water shear stress essentially reduces to

$$\rho_w C_w |\boldsymbol{U}| \boldsymbol{U} = \rho_a C_a |\boldsymbol{U}_a| \boldsymbol{U}_a. \tag{22}$$

Therefore while there is no sea ice in this region, we still compute a velocity which corresponds to satisfying equation (22).

Lastly in Figure 4, we compare the sea ice thickness after 10 years of integration. For comparative purposes we include the sea ice height for three increased P^* values of 5 × 10^4, 7.5 × 10^4 and 1 × 10^5 which is sufficiently high

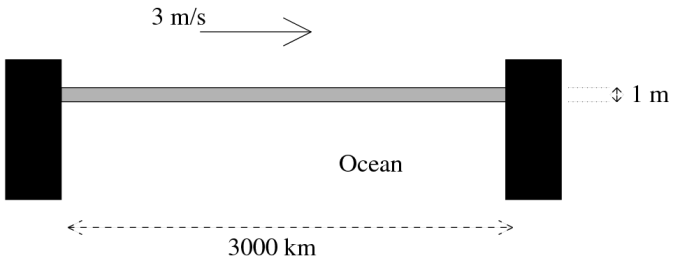

Fig. 2 Illustrative 1D convergent-divergent test problem reproduced here from [13], with air velocity in the -direction forcing the ice to converge on the right coast.

to prevent the creation of open water.

Table 1. 1D test problem simulation parameters

Name	Symbol	Value
Ice density	ρ_i	918 kg m^{-3}
Air density	ρ_a	1.30 kg m^{-3}

Air drag coefficient	C_a	0.0012
Seawater density	ρ_w	1000 kg m^{-3}
Seawater drag coefficient	C_w	0.005
Initial ice thickness	h_0	1 m
Initial ice compactness	A_0	1.0
Air Velocity	$\boldsymbol{U}_a$	8 m s^{-1}

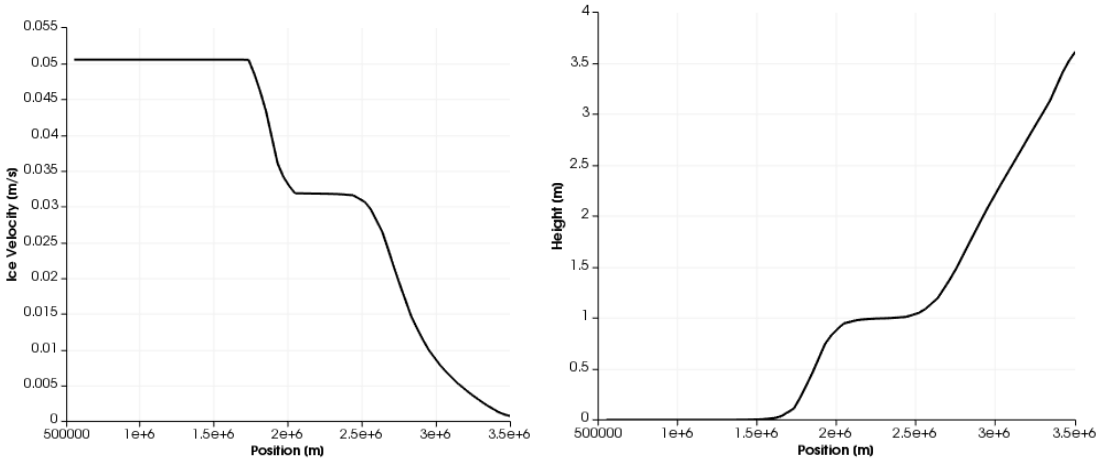

(a) (b)

Fig. 3. 1D-convergence test results after 1 year showing (a) sea ice velocity and (b) sea ice height.

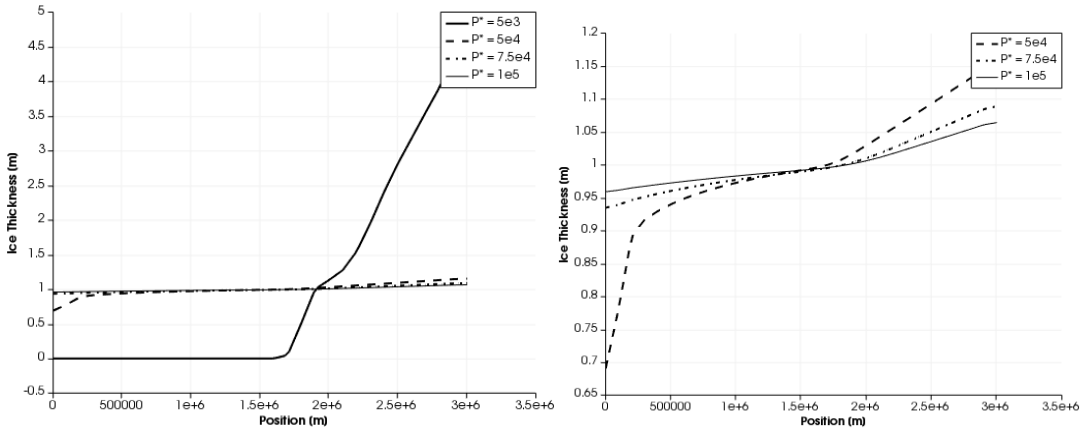

(a) (b)

Fig. 4: Ice thickness for 1D test problem after 10 years, for (a) all 4 ice strengths and (b) with P*=5e3 omitted.

5.2. Wind driven ice

In this section we demonstrate the visco-plastic model on a simple test problem first introduced in [3]. The test problem has been used to great effect to illustrate the difference between various sea ice flow rheologies. The problem layout is illustratively shown in Figure 5, where a 25km by 50km block of ice is subjected to wind forcing and ocean drag. The block of ice is initially at rest, with an initial area coverage fraction of A_0 = 0.9 and ice thickness of h_0 = 2m. The thermodynamic source terms are once again set to zero. A uniform wind surface stress of $\boldsymbol{\tau}_a$ = $(0, -C_a)$ and ocean drag resistance of $\boldsymbol{\tau}_w = -\rho_w C_w \boldsymbol{U}$ are applied, where the simulation parameters are summarized in Table 2. A uniform grid size of 625m is used along with a time step size of Δ = 72s.

A comparison of the sea ice deformation is shown in Figure 6 for both slip and no-slip boundary conditions which compares well to the results presented in [3,19] when using two variations of the finite-element method. The no-slip boundary condition is defined as a boundary condition where the velocity along the boundary is 0, while the slip condition is defined by a 0 velocity in the normal direction to the boundary ($\boldsymbol{U} \cdot \boldsymbol{n}$ = 0) with no tangential stress (i.e. non-zero tangential velocity).

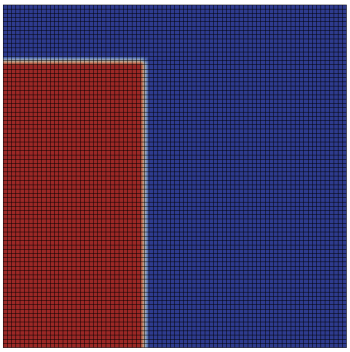

Fig. 5 Visco-plastic flow test problem, with a km block of ice with and .

Table 2. Visco-plastic flow rheology test problem simulation parameters

Name	Symbol	Value
Ice density	ρ_i	918 kg m^{-3}
Air density	ρ_a	1.20 kg m^{-3}
Air drag coefficient	C_a	5 × 10^{-4} m s^{-1}
Seawater density	ρ_w	1026 kg m^{-3}
Seawater drag coefficient	C_w	5 × 10^{-4} m s^{-1}
Initial ice thickness	h_0	2 m
Initial ice compactness	A_0	0.9
Ice strength parameter	P^*	5 × 10^3 kg m^{-1} s^{-2}
Ice strength-compactness parameter	C	15
Eccentricity of ellipse	e	2
Viscosity cut-off	$\zeta_{\max}$	2.5 × 10^8 P s

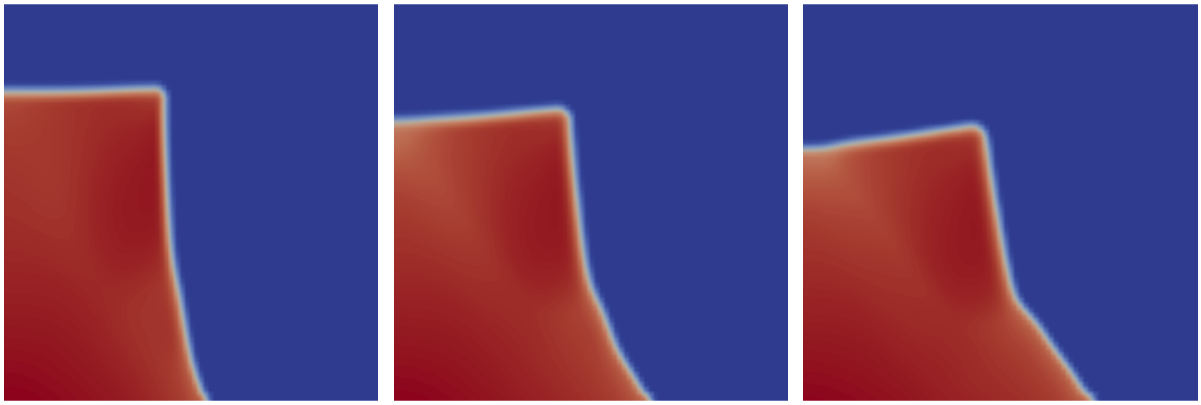

(a) Day 1 (slip boundary) (b) Day 2 (slip boundary) (c) Day 3 (slip boundary)

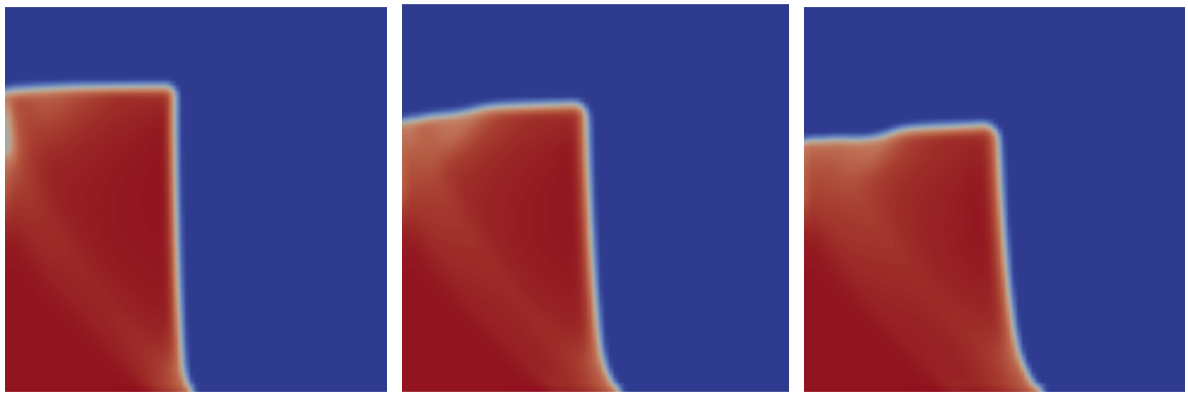

(d) Day 1 (no-slip boundary) (d) Day 2 (no-slip boundary) (f) Day 3 (no-slip boundary)

Fig. 6: Comparison of sea ice deformation over 3 days for (a)-(c) slip and (d)-(f) no-slip boundary conditions.

6. Conclusion

In this paper, we introduced Hibler's visco-plastic model. We illustrated how the convergence rates and solution stability can be improved by combining dynamic relaxation with matrix conditioning. Finally, we demonstrated the VP rheology on two test cases.

[1] Bryan Kirkk, Manabe Syukuro, Pacanowski Ronald C (1975). *A global ocean-atmosphere climate model. Part II. The oceanic circulation*, Journal of Physical Oceanography, 5:30-46.
[2] Campbell, William J (1965). *The wind-driven circulation of ice and water in a polar ocean*, Journal of Geophysical Research, 70:3279--3301.
[3] Schulkes, RMSM and Morland, LW and Staroszczyk, R (1998). *A finite-element treatment of sea ice dynamics for different ice rheologies*, International journal for numerical and analytical methods in geomechanics, 22:153--174.
[4] Hibler III, WD (1979). *A dynamic thermodynamic sea ice model*, Journal of Physical Oceanography, 9:815--846.
[5] Brown, RA (1980). *Planetary boundary layer modeling for AIDJEX*, Sea Ice Processes and Models, :387--401.
[6] McPhee, MG (1975). *Ice-ocean momentum transfer for the AIDJEX ice model*, Aidjex Bull, 29:93--111.
[7] Thorndike, AS and Rothrock, DA and Maykut, GA and Colony, R (1975). *The thickness distribution of sea ice*, Journal of Geophysical Research, 80:4501--4513.
[8] Hutchings, Jennifer K and Jasak, Hrvoje and Laxon, Seymour W (2004). *A strength implicit correction scheme for*

the viscous-plastic sea ice model, Ocean Modelling, 7:111--133.
[9] Lemieux, Jean-Francois and Knoll, Dana A and Tremblay, Bruno and Holland, David M and Losch, Martin (2012). *A comparison of the Jacobian-free Newton--Krylov method and the EVP model for solving the sea ice momentum equation with a viscous-plastic formulation: a serial algorithm study*, Journal of Computational Physics, 231:5926--5944.
[10] Losch, Martin and Danilov, Sergey (2012). *On solving the momentum equations of dynamic sea ice models with implicit solvers and the elastic--viscous--plastic technique*, Ocean Modelling, 41:42--52.
[11] Hunke, EC and Dukowicz, JK (1997). *An elastic--viscous--plastic model for sea ice dynamics*, Journal of Physical Oceanography, 27:1849--1867.
[12] Zhang, Jinlun and Hibler, WD (1997). *On an efficient numerical method for modeling sea ice dynamics*, Journal of Geophysical Research: Oceans, 102:8691--8702.
[13] Hutchings, Jennifer Katy (2000) On modelling the mass of Arctic sea ice, PhD Thesis.
[14] Timmermann, Ralph and Danilov, Sergey and Schröter, Jens and Böning, Carmen and Sidorenko, Dmitry and Rollenhagen, Katja (2009). *Ocean circulation and sea ice distribution in a finite element global sea ice--ocean model*, Ocean Modelling, 27:114--129.
[15] A.E.J. Bogaers and S. Kok and B.D. Reddy and T. Franz (2014). *Quasi-Newton methods for implicit black-box FSI coupling*, Computer Methods in Applied Mechanics and Engineering, 279:113 - 132.
[16] Küttler, Ulrich and Wall, Wolfgang A (2008). *Fixed-point fluid--structure interaction solvers with dynamic relaxation*, Computational Mechanics, 43:61--72.
[17] Bogaers, Alfred Edward Jules (2015) Efficient and robust partitioned solution schemes for fluid-structure interactions, PhD Thesis, University of Cape Town.
[18] HK Versteeg, W Malasekera (2007) An introduction to computational fluid dynamics: the finite volume method.
[19] Sulsky, Deborah and Schreyer, Howard and Peterson, Kara and Kwok, Ron and Coon, Max (2007). *Using the material-point method to model sea ice dynamics*, Journal of Geophysical Research: Oceans, 112.